

Be₂C₅ Monolayer with Quasiplanar Pentacoordinate Carbon Atoms and Ultrahigh Energy Density as a Dirac Anode for Potassium-Ion Batteries

Feilong Wang,¹ Meiling Xu^{✉,†},^{1,*} Shuyi Lin,¹ Jian Hao,¹ Yanchao Wang^{✉,‡},² Hong Jian Zhao,^{2,§} and Yinwei Li^{1,§}

¹ *Laboratory of Quantum Functional Materials Design and Application, School of Physics and Electronic Engineering, Jiangsu Normal University, Xuzhou 221116, China*

² *International Center for Computational Method and Software, State Key Laboratory of Superhard Materials, Key Laboratory of Physics and Technology for Advanced Batteries, Ministry of Education, College of Physics, Jilin University, Changchun 130012, China*



(Received 24 May 2023; revised 7 July 2023; accepted 20 July 2023; published 24 August 2023)

K-ion batteries (KIBs) are of potential importance in the future energy industries. Recent efforts were committed to increasing the energy storage density in KIBs. Here, we search for anode materials with high energy density that are compatible with KIBs, by a combination of the swarm-intelligence structure search method and first-principles calculations. We predict the Be₂C₅ monolayer to be a kind of material that showcases ultrahigh energy density (~5455 mWh/g, referenced to the standard hydrogen electrode potential), thanks to an exceptional specific capacity of 2060 mAh/g and low average open-circuit voltage of 0.28 V. This energy density value is much larger than that of most currently known 2D KIB-based anode materials. Furthermore, the Be₂C₅ anode presents other intriguing behavior, such as (i) the fast diffusion of K ions, as suggested by an ultralow barrier energy of about 0.074 eV; (ii) excellent mechanical strength, with a Young's modulus of about 243 N/m; (iii) robust compatibility with electrolytes; (iv) small-scale volume expansion of 0.68% during the process of potassiation; and (v) a unique “self-doping” effect, which is beneficial for high electronic conductivity.

DOI: 10.1103/PRXEnergy.2.033012

I. INTRODUCTION

Over the last decades, the exploitation and utilization of renewable and green energy sources has become one of the most urgent research directions [1]. Rechargeable Li-ion batteries (LIBs) with a high specific capacity and long cycle life [2] are energy storage materials that are important and promising for portable and wearable electronic devices, electronic and hybrid vehicle systems, etc. [3]. Nonetheless, the application scope for LIBs in large-format storage systems is limited by the scarcity and uneven distribution of lithium resources [1]. A possible avenue to overcome the aforementioned shortcomings of LIBs is the development of novel battery materials

(i.e., replacing LIBs) that are based on K, Na, or Mg ions due to their abundance and potential cost-effectiveness [4–7]. Among them, K-ion batteries (KIBs) are competitive and attract enormous attention [8]. The K ion has a smaller Stokes radius than Li, yielding higher ion mobility and conductivity when transferring across liquid-solid interfaces (i.e., the solvation shell effects [9]). To appreciate high-performance KIB-based devices, advanced anode materials are critical [10], as anode materials are typically not interchangeable between LIBs and other types of batteries [11].

The family of standard KIB anode materials can basically be categorized into three distinct types [12]: (i) intercalation type, including graphite, other carbon-based materials, and layered transition metal chalcogenides [13]; (ii) conversion type, as represented by, e.g., transition metal oxides and sulfides [14,15]; and (iii) alloy type, containing Bi, Sn, and their derivatives [16–18]. Typically, the intercalation-type and alloy-type anodes have low capacity (<385 mAh/g), and the conversion-type anodes showcase a high discharge platform (>0.8 V), which is detrimental to achieving a high energy density for KIB anodes [19,20]. Therefore, efforts should be made toward the exploration of new types of anode materials and new strategies [21] for improving the energy density of KIBs. In this regard,

*xuml@jsnu.edu.cn

†xml@calypso.cn

‡physzhaohj@jlu.edu.cn

§yinwei_li@jsnu.edu.cn

two-dimensional (2D) materials are potential candidates for anode materials towards KIBs; such materials are not only abundant raw materials but also have suitable mechanical strength, chemical stability, and high specific surface area [22]. This family of 2D materials contains transition metal carbides or nitrides (MXenes) [23–25], transition metal dichalcogenides [7,26,27], carbon-based materials [28–45] (e.g., C₄S [28], BC₃ [31], BC₆P [33], C₃₆H₈ [35], and C₃N [43]), and 2D Dirac materials [46–56] (e.g., B₂S [46], BH [47], Be₂P₃N [48], B₃F [49], B₂P₂ [50], and BeN₄ [51]). Of particular interest is 2D materials with a Dirac cone, demonstrating inherently high electrical conductivity and robust surface states, which have charge-discharge channels for enhanced rate capability [46,57]. Overall, the energy density in these 2D Dirac materials is moderate (e.g., 3325 mWh/g in Be₂P₃N [48], 3059 mWh/g in BH [47], 1167 mWh/g in B₂S [46]), much smaller than that of 4787 mWh/g in borophene [48,58] and 5383 mWh/g in C₄S [28].

Here, we designed an anode material for KIBs with ultrahigh energy density by considering a class of compounds with a Dirac cone in band structures. Using a swarm-intelligence structure search method and first-principles calculations, we focused on Be–C monolayers with a high carbon content and carried out an extensive computational study. We found a desired Dirac anode material, Be₂C₅, for KIBs with an energy density up to 5455 mWh/g, a product with a high specific capacity of 2060 mAh/g, and a low average open-circuit voltage (OCV) of 0.28 V. Additionally, the Be₂C₅ anode presents (i) a diffusion energy barrier (for K-ion migration on the Be₂C₅ surface) as low as 0.074 eV; (ii) a Young's modulus of about 243 N/m; (iii) a robust compatibility with electrolytes; (iv) a volume expansion as small as about 0.68% during the process of potassiation; and (v) a unique “self-doping” effect arising from the emergence of the Be vacancy in Be₂C₅, enhancing the electronic conductivity.

II. COMPUTATIONAL METHODS

Crystal structures of Be_xC_y ($x = 1, y = 1\text{--}5; x:y = 2:3, 2:5; x = 2\text{--}5, y = 1; x:y = 3:2, 5:2$) monolayers (involving four formula units at most) were predicted by CALYPSO [59–63]; this is a method and software extensively used for structural predictions [64–69]. First-principles calculations were conducted by using the Vienna *ab initio* simulation package [70], with (i) the exchange-correlation functional being specified as the generalized gradient approximation parameterized by Perdew, Burke, and Ernzerhof [71]; and (ii) the electron-ion interactions being described by the projector augmented plane wave approximation ($2s^2$ for Be and $2s^22p^2$ for C) [72]. The plane wave cutoff energy was set to 550 eV, and the Monkhorst-Pack k -point grid was selected as $5 \times 7 \times 1$ (with respect to the cell containing two formula units) during the self-consistent

calculation. Such settings give well-converged total energies and forces. During the calculation of the density of states, the k -point grid was further increased to $35 \times 49 \times 1$. The monolayers were mimicked by the periodic cell with a large vacuum thickness of 30 Å along the out-of-plane direction. The dynamic stability was investigated by phonon calculations via the finite displacement method, as implemented in PHONOPY code [73]. Thermal stability was further confirmed by *ab initio* molecular dynamics (MD) simulations based on a $2 \times 3 \times 1$ supercell. Temperatures of 300, 800, and 1500 K were examined using a Nosé-Hoover chain thermostat with a total simulation time of 10 ps (time step of 1 fs). The van der Waals effects were considered by the DFT-D3 method [74] during the calculations of adsorption energy. The climbing image nudged elastic band method [75,76] was employed to locate the minimum-energy pathway between the given initial and final configurations; this also allowed the estimation of energy barriers for K-ion diffusion. Finally, computational details regarding the Young's modulus, Poisson's ratio, Fermi velocity, adsorption energy, temperature-dependent molecular diffusion constant, OCV, formation energy, specific capacity, and lattice change rate are provided in the Supplemental Material [77].

III. RESULTS AND DISCUSSION

A. Structure and stability of the Be₂C₅ monolayer

Our structure search indicates the *P2/c* phase as the lowest energy structure of the Be₂C₅ monolayer. As shown in Fig. 1(a) and Table SI within the Supplemental Material [77], the lattice constants of this phase are $a = 7.33$ Å and $b = 4.99$ Å. The basic building block of the Be₂C₅ monolayer is the 1,5-dimethylnaphthalene unit and armchair-type Be–Be chain [Fig. 1(b)]. Within this building block, all C atoms are in the same plane, while Be atoms are situated on either side of the partial C atoms. Each Be atom connects three neighboring C atoms, with an average Be–C bond length of 1.78 Å; the C atoms in the methyl group position bind with four Be atoms and another C atom in almost the same plane, forming a quasiplanar pentacoordinate carbon moiety. The average length of the C–C bond is 1.44 Å, which is comparable to that of 1.42 Å in graphene [103]. Figure 1(c) is the electron localization function [104] of Be₂C₅, which is linked to the bonding nature. The obvious electron localization between the nearest-neighbor C atoms and that between Be and C atoms imply a strong covalent interaction. Bader charges analysis [105] further shows that each Be atom transfers $1.60 |e|$ (e is the elementary charge) to the C atom. Therefore, the Be₂C₅ monolayer simultaneously exhibits covalent, ionic, and metallic bonds.

To address the stability of the *P2/c* phase, we performed phonon calculations and MD simulations. As shown in Fig. S1(a) within the Supplemental Material [77], the

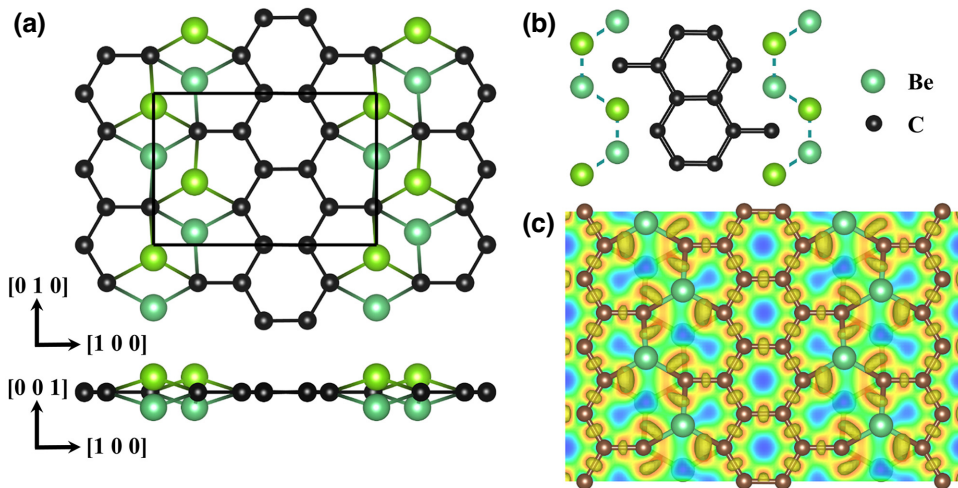


FIG. 1. (a) Top and side views of the geometric structure of the Be₂C₅ monolayer with a unit cell marked by black solid lines. Green and black spheres are Be and C atoms, respectively. (b) 1,5-Dimethylnaphthalene unit and armchair-type Be–Be chain in the Be₂C₅ monolayer. (c) Electron localization function map of the Be₂C₅ monolayer with an isovalue of 0.85 e/bohr³.

phonon spectrum confirms the dynamic stability of the Be₂C₅ monolayer, as evidenced by the absence of imaginary frequencies in the entire Brillouin zone. In the MD simulations, the Be₂C₅ monolayer still can retain its structural integrity (without relevant distortions) after being heated at a maximum of 1500 K for 10 ps; this is further confirmed by the small energy fluctuation [Figs. S1(b) and S2 within the Supplemental Material [77]]. In addition, the calculated elastic constants of the Be₂C₅ monolayer (Table SII within the Supplemental Material [77]) meet the Born criteria [106] for 2D systems, implying mechanical stability. The direction-dependent Young's modulus and Poisson's ratio along an arbitrary direction θ (θ is the angle relative to the positive x direction in the sheet) are then obtained based on the elastic constants [Figs. S1(c) and S1(d) within the Supplemental Material [77]]. The degree of anisotropy of the Young's modulus of the Be₂C₅ monolayer is relatively small. The maximum Young's modulus is 243 N/m, which is less than that (342 N/m) of graphene [107] and *h*-BN (275.8 N/m) [108]. On the other hand, our calculated value is much larger than that of silicene (62 N/m) [109] and the MoS₂ monolayer (129 N/m) [110]. This basically can be interpreted by the presence of strong C–C covalent bonds in the Be₂C₅ monolayer.

B. Electronic properties of the Be₂C₅ monolayer

Figure 2(a) shows the electronic band structure and projected density of states (PDOS) for the Be₂C₅ monolayer. The band gap is closed at the Fermi level with a band-crossing point (i.e., the 2D Dirac point) located along the X – S high-symmetric line in the Brillouin zone. This is different from the case in graphene, the Dirac point of which is at the K and K' points. Indeed, the lattice structure of the Be₂C₅ monolayer is not a honeycomb. The existence

of the Dirac point in the nonhoneycomb lattice can also be found in 1*H'*-MoS₂ [111], B₂Se [112], B₂S [113], and borophosphene [114]. As shown in Fig. 2(c), the Dirac points are mainly contributed to by the p_z orbitals of C atoms. The band structure calculated with the HSE06 functional [115] still showcases such a Dirac point [Fig. 2(a)]. Involving the spin-orbit coupling (SOC) effect does not obviously change the band structure [Fig. 2(b)], revealing the weak SOC nature in the Be₂C₅ monolayer. Therefore, our calculations are based on the PBE functional, ignoring the SOC effect. Our calculated Fermi velocity of the Be₂C₅ monolayer (around the Dirac points) is about 5.15×10^5 and 4.98×10^5 m/s along the k_x and k_y directions, respectively, implying the anisotropy of the Fermi velocities. Such Fermi velocities are of the same order of magnitude as that (8.2×10^5 m/s) in graphene [116]. The existence of the Dirac cone at the Fermi level in the Be₂C₅ monolayer could facilitate charge transport and, in turn, improve the charging-discharging rate.

C. K-ion adsorption and migration

We move on to discuss the adsorption and migration of K ions in the Be₂C₅ monolayer, since these properties are related to the performance of the anode material in alkali-metal-ion batteries. To this end, eight possible adsorption sites with high geometric symmetry are considered (Fig. S3 within the Supplemental Material [77]). Our simulations are carried out within the $2 \times 2 \times 1$ supercell (Be₁₆C₄₀), to avoid interactions between adjacent metal atoms (the distances are 9.97 and 14.68 Å along the a and b directions, respectively). After full structural relaxation, it was observed that there were only four adsorption sites. The results of the adsorption tests are summarized in Fig. 3(a) and Table SIII within the Supplemental Material

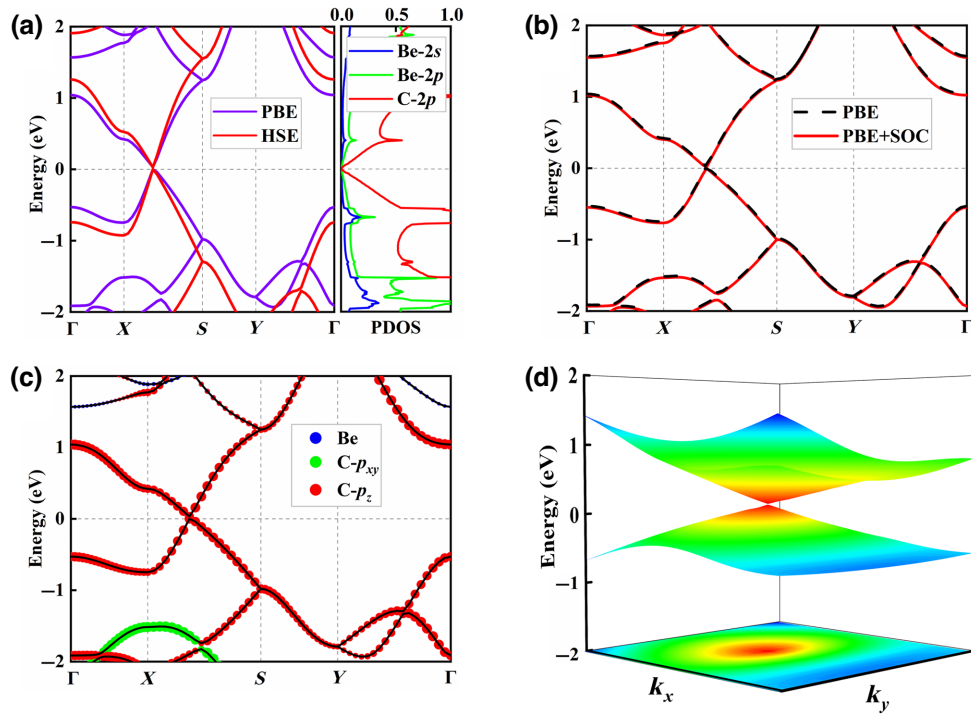


FIG. 2. (a) Electronic band structure and projected density of states of the Be₂C₅ monolayer at the PBE level. Band structure is also calculated by using the HSE06 functional. (b) Comparison of the band structure of the Be₂C₅ monolayer with and without the SOC effect. (c) Projected band structure of the Be₂C₅ monolayer. (d) Three-dimensional band structure and projection showing a Dirac point. Fermi level is set to zero.

[77]. A positive adsorption energy implies that the metal atoms prefer to form metallic dendrites or clusters rather than staying separately on the Be₂C₅ monolayer. Such an aspect excludes the Be₂C₅ monolayer from being an anode material for Li- and Na-ion batteries [see Fig. 3(a)]. Strikingly, the adsorption energies of the K atoms on these sites are negative, ranging from -0.47 to -0.39 eV. Such values are large enough to prevent the formation of metallic dendrites. The adsorption of a K atom preserves the Dirac point and shifts it toward deeper energy levels [Fig. 3(b)]. This is understandable from the Bader charge analysis, which shows that the K atom transfers 0.87 |e| to the Be₂C₅ monolayer. This is also supported by the charge density difference plot [Fig. 3(c)]. Figure 3(d) illustrates the PDOS, indicating a significant overlap between the C-2p and K-3p orbitals below the Fermi level (i.e., a strong interaction). This suggests that both orbital hybridization and electron transfer are crucial factors in the adsorption of K.

Another vital index to assess the suitability of anode materials is the rate performance, which positively correlates to the mobility of the K ion. To appreciate the mobility of K ions, diffusion pathways for metal-ion migration are chosen for linking the most energetically favorable site of K to its equivalent nearest site. Here, we select three paths [marked as path I, path II, and path III in Figs. 4(a)–4(c)]. For path III, the metastable adsorption position (H1) is considered as a possible middle state. Using the

climbing image nudged elastic band method, we calculate the diffusion energy barrier for K-ion migration. Path III suggests the lowest energy barrier (0.074 eV) for K-ion migration, which is much lower than those of most 2D materials [see Fig. 5(a) and Table SIV within the Supplemental Material [77]], such as BP (0.155 eV) [91], Si₃C (0.18 eV) [36], C₆S (0.11 eV) [28], BC₆P (0.13 eV) [33], BC₃ (0.12 eV) [31], PC₅ (0.18 eV) [56], and C₅N (0.11 eV) [29]. The temperature-dependent molecular diffusion constant based on transition state theory can be used to evaluate the charge-discharge rate. At room temperature (300 K), the diffusion constant of K ions along path III is approximately 5.7×10^{-2} , which is larger than that in C₆S (1.4×10^{-2}) [28] and BC₆P (6.5×10^{-3}) [33].

D. Specific capacity, average OCV, energy density, and durability

Theoretically, the number of adsorbed atoms determines the specific capacity of anode materials. In such a sense, the relationship between the adsorption concentration and behavior of metallic K on the Be₂C₅ monolayer can be studied by adsorbing multiple metal K atoms on both sides of Be₂C₅. In the present work, six different concentrations of K atoms (i.e., Be₂C₅K_x, $x = 1\text{--}6$) are considered by gradually loading on both sides of the $2 \times 2 \times 1$ supercell (Be₁₆C₄₀) layer by layer.

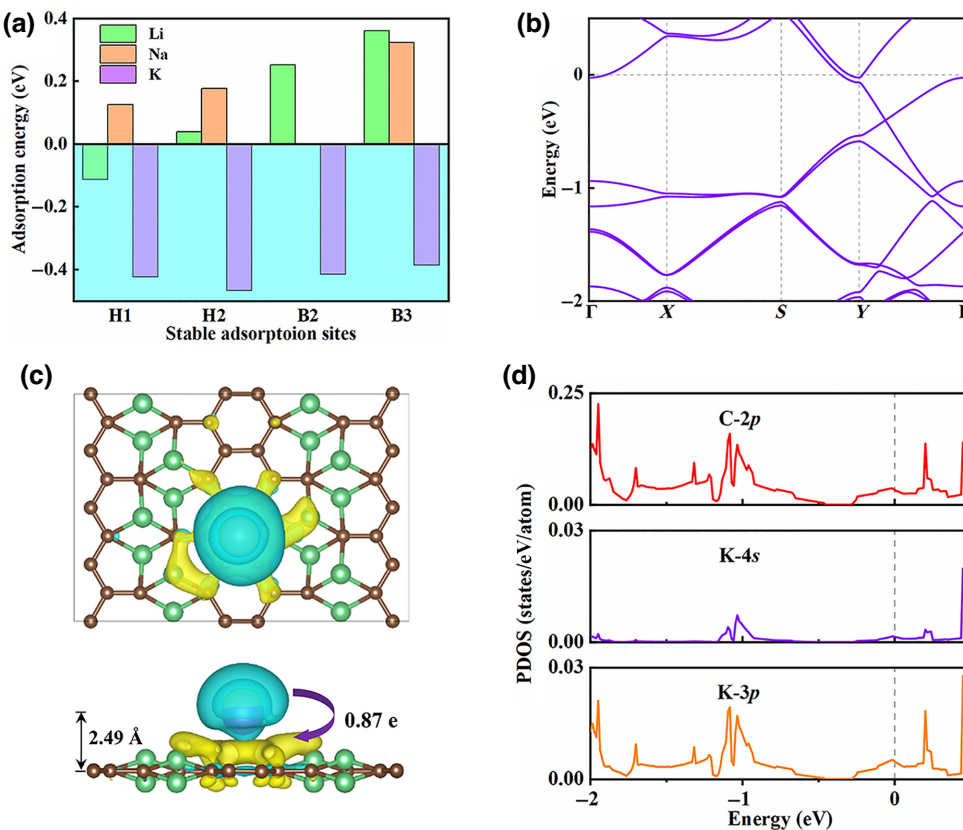


FIG. 3. (a) Adsorption energies (E_{ad}) of Li, Na, and K ions at different stable adsorption sites of the Be₂C₅ monolayer. (b) Band structure, (c) charge density difference, and (d) PDOS of K ion adsorbed at the most favorable site of the Be₂C₅ monolayer. Fermi level is set to zero and indicated by dashed lines. Blue and yellow areas indicate electron depletion and accumulation, respectively. Isosurface value is considered to be 0.001 e/bohr³.

The average adsorption energy (E_{av}) and the layer-by-layer average adsorption energy ($E_{av-layer}$) were calculated to examine the storage performance of K metal of the Be₂C₅ monolayer. When the adsorption energy becomes positive or convergent with the increased metal K concentrations, the maximum specific capacity can be determined. As shown in Figs. 4(d) and 4(e), the adsorption energy decreases with the increase of K adatoms, owing to the repulsion forces of neighboring K adatoms. The calculated results indicate that a maximum of 48 atoms can be accommodated on both sides of the Be₂C₅ monolayer. In other words, a total of three layers with eight atoms per layer on one side can be formed with the corresponding stoichiometric ratio of Be₂C₅K₆. Accordingly, the theoretical specific capacity is calculated to be as high as 2060 mAh/g. Such a value is the highest among the reported 2D materials [Fig. 5(b) and Table SIV within the Supplemental Material [77]]. This implies that the Be₂C₅ anode is capable of storing plenty of energy.

To evaluate the relative stability of Be₂C₅K_x, we construct the convex hull diagram of formation energy concerning the Be₂C₅ and Be₂C₅K₆ phases. Together with

the reference Be₂C₅K₆ phase, we find two thermodynamically stable intermediate phases (Be₂C₅K₂ and Be₂C₅K₄) lying on the convex hull [Fig. 4(f)]. After multiple K atoms are adsorbed, the three stable structures remain metallic (Fig. S4 within the Supplemental Material [77]) with appropriate electronic conductivity in the charging-discharging process. The fully metallized phases must possess sufficient thermal stability without metal ion desorption, clustering, and irreversible electrode deformation. Our MD simulations at 300 K for 8 ps demonstrate that the Be₂C₅ monolayer is slightly distorted when multiple K atoms are adsorbed. This is attributed to good mechanical strength (Fig. S5 within the Supplemental Material [77]). Furthermore, the K atoms in Be₂C₅K_x ($x = 2, 4$, and 6) are not pushed out of the anode or clustered, indicating the thermally stable nature of these materials. The maximum K adsorption concentration corresponds to Be₂C₅K₆, in which the Be₂C₅ monolayer adsorbs three-layer K atoms on both sides. After the removal of all K atoms from the Be₂C₅ surface, we rerun the MD simulations and find that the slightly deformed Be₂C₅ monolayer can quickly recover its initial configuration (Fig. S5 within the Supplemental Material [77]). These aforementioned calculations

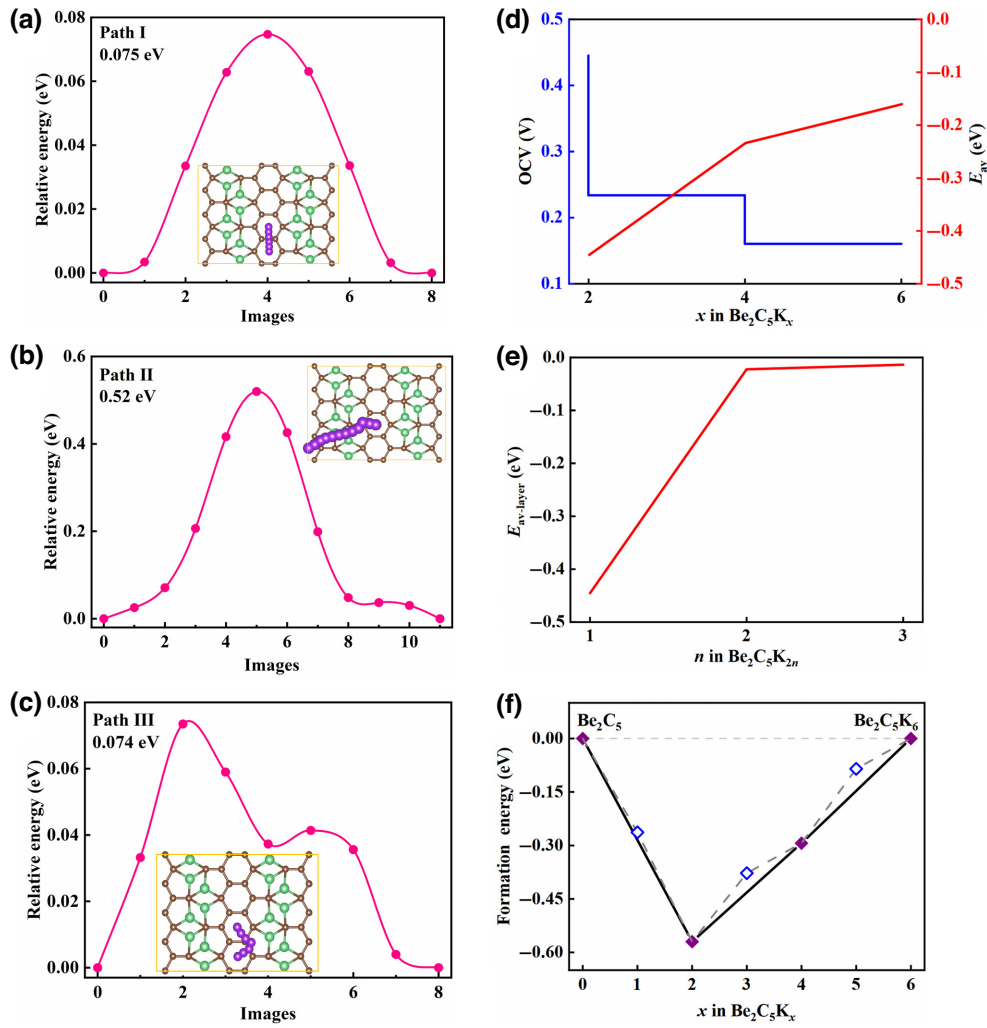


FIG. 4. (a)–(c) Optimized potassium diffusion pathway and the corresponding energy barrier on the Be_2C_5 monolayer. (d) Calculated OCVs and average adsorption energy (E_{av}) of K ions on the Be_2C_5 monolayer as the number of adsorbed metal atoms (x) increases. (e) Calculated layer-by-layer average adsorption energy ($E_{av-layer}$) of K ions on the Be_2C_5 monolayer as the number of adsorbed layers (n) increases. For instance, $n = 1$ represents a total of 16 K atoms being adsorbed on both sides of Be_2C_5 (eight K atoms on one side), corresponding to the stoichiometry of $\text{Be}_2\text{C}_5\text{K}_2$. (f) Convex hull diagram of the formation energies of $\text{Be}_2\text{C}_5\text{K}_x$ ($x = 1$ –6) concerning Be_2C_5 and $\text{Be}_2\text{C}_5\text{K}_6$. Solid and hollow squares represent thermodynamically stable and unstable structures, respectively.

reveal the good phase stability of the Be_2C_5 monolayer during the K-ion insertion-extraction processes.

Considering $\text{Be}_2\text{C}_5\text{K}_x$ ($x = 2$, 4, and 6), we then computed their average OCVs. The average OCV value of Be_2C_5 for K storage versus the metal electrode is 0.28 V, which is comparable to that of commercial graphite for LIBs [117] and smaller than those in BC_2P (0.44 V) [33] and BC_6P (0.35 V) [33]. We also calculated the average OCV for K, regarding other $\text{Be}_2\text{C}_5\text{K}_x$ structures ($x = 1$, 3, and 5). The average OCV is estimated to be 0.288 V (Fig. S6 within the Supplemental Material [77]), which is quite close to that for $\text{Be}_2\text{C}_5\text{K}_x$ ($x = 2$, 4, and 6). Additionally, the decreasing trend of OCVs (when increasing the K concentration) is a fantastic advantage [Figs. 4(d) and 4(e)]. This is evidenced by a small OCV value

providing a higher working voltage and energy density for rechargeable batteries when it is coupled with a cathode material.

The energy density, which is a crucial parameter to assess the electrochemical performance of anode materials, can be calculated as the product of specific capacity and average OCV. For such a calculation, the standard hydrogen electrode potential (SHE) is used as the universal cathode reference potential in these evaluations [118]. Typically, a combination of high specific capacity and low average OCV yields high energy density. Here, the energy density, D , is estimated from the average OCV (V_{av}), the specific capacity (C), and the relative potential of -2.928 V versus SHE for K as $D = [-2.928 \text{ V} \text{ versus SHE} + V_{av}] \times C$. Our calculated energy

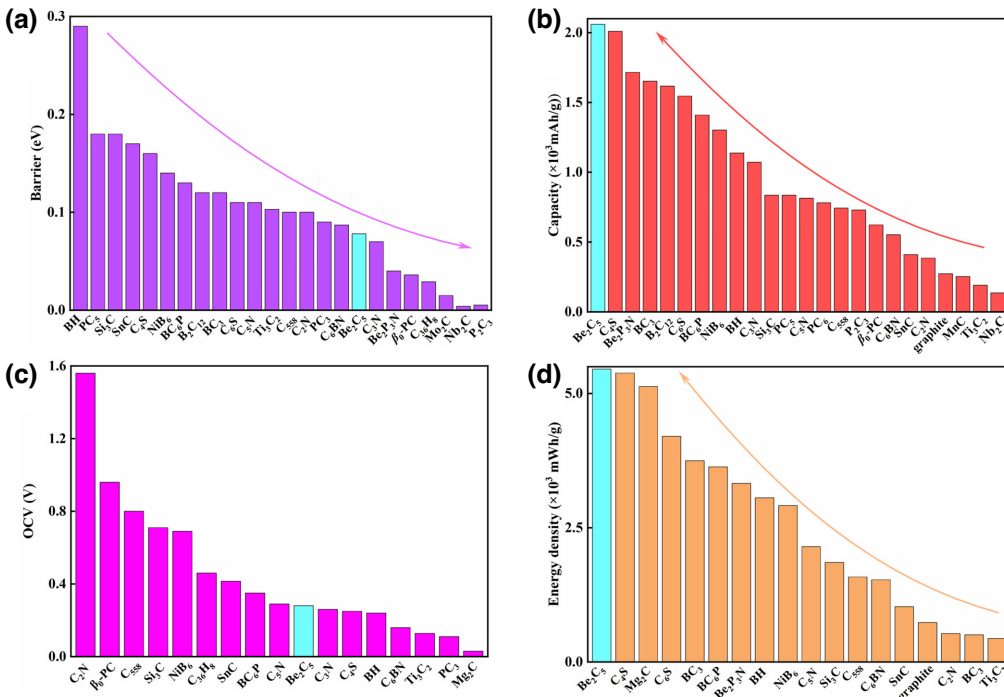


FIG. 5. Summaries of the (a) diffusion barrier, (b) theoretical specific capacity, (c) average OCV, and (d) energy density of the Be_2C_5 monolayer and other 2D materials for KIBs. Please see Table SIV within the Supplemental Material [77] for an exhaustive comparison with other 2D materials.

density in the Be_2C_5 anode is 5455 mWh/g. Such a value is quite high among all previously reported 2D anode materials [as shown in Fig. 5(d) and Table SIV within the Supplemental Material [77]]. This impressive value indicates that Be_2C_5 has great potential for storing a substantial amount of energy in KIBs.

We also computed the volume change rate for $\text{Be}_2\text{C}_5\text{K}_2$, $\text{Be}_2\text{C}_5\text{K}_4$, and $\text{Be}_2\text{C}_5\text{K}_6$, which were 0.45%, 0.55%, and 0.68%, respectively. These values are much smaller than that of commercialized graphite anode material intercalated with Li (12%) [119] and lower than those of most 2D materials, such as Si_3C (0.97%) [36], B_2S (2%) [46], and BH electrode (1.85%) [47]. The small volume variation can prevent electrode fracture and specific capacity fading of the materials [120,121].

E. Compatibility between typical electrolytes and the Be₂C₅ anode

Now, we discuss the compatibility between typical electrolytes and the Be_2C_5 anode, a crucial factor for the assessment of the overall performance and stability of the battery system [122]. For this purpose, we selected several commonly used electrolytes [123–125] in K-ion batteries and assessed the compatibility between the Be_2C_5 anode and these electrolytes. The chosen electrolytes encompass solvent molecules, such as diethyl carbonate (DEC), dimethyl carbonate (DMC), ethylene carbonate (EC), and propylene carbonate (PC), and metal salts (e.g., KPF_6 , KFSI , and KTFSI). Notably, the compatibility between electrolytes and the Be_2C_5 surface can be evaluated from the adsorption energy (E_{ad}) of the electrolytes to the

Be_2C_5 surface. In particular, we examined several different adsorption configurations and determined the most energetically favorable one (see Figs. S7 and S8 within the Supplemental Material [77]), for identifying the most stable adsorption site for the electrolytes on the Be_2C_5 surface. The results are tabulated in Table I. Overall, the calculated adsorption energies (E_{ad}) of all the considered solvent molecules exhibit negative values, ranging from -1.17 to -1.41 eV, implying the strong interaction between the solvent molecules and the Be_2C_5 surface. In contrast to the solvent molecules, the binding between the metal salt and the Be_2C_5 surface is considerably stronger, as evidenced by their higher adsorption energies (E_{ad}), ranging from -1.66 to -2.36 eV [Table I]. Remarkably, the adsorption energies of DMC, EC, and PC molecules on Be_2C_5 are approximately twice those of graphene and B_2S [46]. This suggests the superior wettability of Be_2C_5 and a

TABLE I. Comparison of the adsorption energies of the solvent molecules DEC, DMC, EC, and PC, as well as metal salts KPF₆, KFSI, and KTFSI, on Be₂C₅, graphene, and B₂S anodes.

		E_{ad} (eV)		
Electrolytes		Be_2C_5	Graphene	B_2S
Solvent molecule	DEC	-1.41	-0.87	-0.69
	DMC	-1.18	-0.54	-0.44
	EC	-1.17	-0.56	-0.51
	PC	-1.30	-0.69	-0.63
Metal salt	KPF ₆	-1.66	-1.39	-0.92
	KFSI	-2.23	-1.61	-1.10
	KTFSI	-2.36	-1.56	-0.92

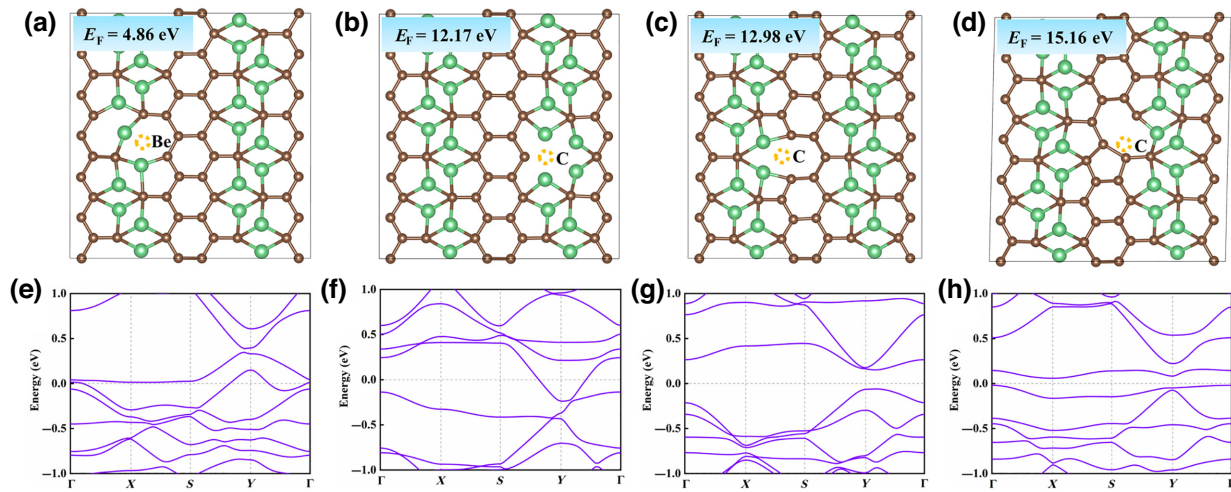


FIG. 6. Relaxed structures of the 2×3 Be_2C_5 supercell with various vacancies, including (a) Be vacancy, (b) CI vacancy, (c) CII vacancy, and (d) CIII vacancy. Corresponding electronic band structures are presented in (e)–(h) for each vacancy configuration.

more favorable wetting process, even without the addition of metal salts.

F. The mechanical performance of graphene- Be_2C_5 composite anodes

In this section, we show the mechanical properties of the graphene- Be_2C_5 composite anodes. We select graphene as a supplementary anode for pure Be_2C_5 ; note that graphene is a frequently used supportive matrix for other functional materials or as a vital constituent in composite materials. The lattice mismatches for the Be_2C_5 -(4 \times 1)/rectangle graphene-(7 \times 2) composite are 1.7% and 1.4% along the x and y directions, respectively (Fig. S9 within the Supplemental Material [77]). The calculated elastic constants of the pure monolayer Be_2C_5 , bilayer Be_2C_5 , and graphene- Be_2C_5 composite are shown in Table SII within the Supplemental Material [77]. The elastic constants of bilayer Be_2C_5 and graphene- Be_2C_5 composite meet the Born criteria for 2D systems, implying mechanical stability. The graphene- Be_2C_5 composite exhibits greater in-plane stiffness ($E_x = 567.06$ N/m and $E_y = 574.91$ N/m) when compared to the pure monolayer ($E_x = 243.13$ N/m and $E_y = 237.61$ N/m), and bilayer Be_2C_5 ($E_x = 483.63$ N/m and $E_y = 471.34$ N/m). The stress-strain curves for both pure monolayer Be_2C_5 and the graphene- Be_2C_5 composite were computed along the x and y directions to facilitate a comparison of their elastic limits. As shown in Fig. S10 within the Supplemental Material [77], the graphene- Be_2C_5 composite exhibits an impressive ultimate tensile strength of 45 N/m along the y direction and 40 N/m along the x direction. These values surpass the corresponding ultimate tensile strengths of pure monolayer Be_2C_5 , which are 28 and 21 N/m along the y and x directions, respectively. We also investigated the effect of potassiation on

the mechanical properties of the Be_2C_5 anode. The in-plane stiffness of Be_2C_5 gradually decreases as the number of K adatoms increases. For example, the Young's modulus along the x direction decreases to 223.09 N/m for $\text{Be}_2\text{C}_5\text{K}_4$. Such a value is still higher than that of many other 2D materials, such as MoS_2 (123 N/m) and phosphorene (91.3 N/m). In other words, both the graphene- Be_2C_5 composite anode and the pure Be_2C_5 anode (even after potassiation) exhibit favorable mechanical strength.

G. Possibility for synthesizing the Be_2C_5 monolayer

We now assess the possibility of synthesizing the Be_2C_5 monolayer by calculating its cohesive energy, $E_{coh} = (2E_{\text{Be}} + 5E_{\text{C}} - E_{\text{Be}_2\text{C}_5})/7$, where $E_{\text{Be}_2\text{C}_5}$ is the total energy of the Be_2C_5 monolayer and E_{C} and E_{Be} are the energies of isolated C and Be atoms, respectively. Here, a more positive E_{coh} value indicates higher thermodynamic stability. The calculated E_{coh} of the Be_2C_5 monolayer is 7.26 eV/atom, which is comparable to or higher than those of Be-C (4.82–4.58 eV) [68,126], B_2S (5.3 eV) [113], C_4S (7.26 eV) [28], and borophosphene [114] (4.82 eV) monolayers. The relatively high cohesive energy suggests the strongly bonded network in the Be_2C_5 monolayer. Notably, well-synthesized graphene has a cohesive energy of 0.69 eV/atom. Our calculated results thus imply the feasibility of synthesizing the Be_2C_5 monolayer. Since there is no natural parent structure for Be_2C_5 in a layered form, a promising approach to obtain this material may be through growth of the Be_2C_5 monolayer on a suitable substrate via chemical vapor deposition or molecular beam epitaxy methods with an accurately controlled Be : C ratio. As Be element is highly toxic and the synthesis of the Be_2C_5 monolayer may require high temperature, special safety precautions must be taken (e.g., without exposure to Be) during the synthesis process. We recall that the solid

forms of Be-based materials (such as BeC, BeO, BeCu, and BeAl) are generally considered to be nontoxic materials. In such a sense, the development of effective recycling methods for batteries that use Be-containing compounds as electrode materials remains promising.

H. The effect of lattice defects on the properties of the Be₂C₅ monolayer

For the completeness of our discussion, we investigated the influence of lattice vacancies on the properties of the Be₂C₅ monolayer. To create the vacancies, we removed a Be or a C atom from a 2 × 3 supercell (initially containing 24 Be and 60 C atoms), resulting in a vacancy concentration of 1.2%. Upon structural optimization, we found that the presence of a Be vacancy defect did not lead to significant local atomic reconstruction [see Fig. 6(a)]. In contrast, the C vacancies exhibit a relatively substantial impact on the local atomic reconstruction, as illustrated in Figs. 6(b)–6(d). The formation energy of a defect, determining the possibility of its existence in Be₂C₅, can be calculated by

$$E_F = E_{\text{defect}} + E_{\text{Be/C}} - E_{\text{Be}_2\text{C}_5},$$

where E_{defect} and $E_{\text{Be}_2\text{C}_5}$ are the total energies of the defective and intrinsic Be₂C₅ monolayer, respectively. Also, $E_{\text{Be(C)}}$ represents the energy of an isolated Be (C) atom. Our calculated formation energy for the Be vacancy is 4.86 eV, which is smaller than that (12.17–15.16 eV) of C vacancies, indicating that the Be vacancy defect forms more easily. The difficulty of creating a C vacancy in the honeycomb C framework implies that the π -electron network along the [010] direction cannot be easily destroyed. Therefore, the Dirac state in the pure Be₂C₅ monolayer can likely be preserved, even in the presence of vacancies. Additionally, the creation of a Be vacancy does not induce magnetism, different from graphene with vacancy defects. Electronic band structures show that p -type doping could be obtained by forming a Be vacancy, leading to a unique self-doping effect, as illustrated in Fig. 6(e). This self-doping effect is also observed in the B₂S Dirac anode material with lattice vacancies [46]. Such an effect is conducive to achieving high electronic conductivity without the aid of extra conductive additives.

To further explore the potential of defective Be₂C₅ monolayers as an anode material, we conducted investigations into the formation energies on the Be₂C₅ monolayer, adsorbed with 1 and 48 K atoms. The adsorption energies associated with the adsorption of 1 and 48 K atoms are –1.51 and –0.19 eV, respectively. These values indicate that K atoms exhibit favorable adsorption on the defective Be₂C₅ anode. This implies that the presence of defects in the Be₂C₅ monolayer has a negligible influence on its performance as an anode material.

IV. CONCLUSIONS

We predicted, via a combination of the CALYPSO method and first-principles calculations, a new thermodynamically stable Be₂C₅ monolayer as a promising anode material for KIBs. The Be₂C₅ monolayer exhibited a distinctive structure consisting of two components: a 1,5-dimethylnaphthalene unit and an armchair-type Be–Be chain. Within this structure, a C atom positioned on the methyl groups was quasiplanar pentacoordinated. Electronic properties calculations revealed the occurrence of an anisotropic Dirac cone originating from C- p_z orbitals. Strikingly, the Be₂C₅ monolayer had an ultrahigh specific capacity of 2060 mAh/g and a low average OCV of 0.28 V, yielding an energy density of 5455 mWh/g. Furthermore, the Be₂C₅ monolayer exhibited a low energy barrier of 0.074 eV for K-ion migration, a small-scale volume expansion of 0.68% during the process of potassiation, a Young's modulus up to 243 N/m, and high thermal stability. Meanwhile, the Be₂C₅ anode possessed excellent compatibility with the contacted electrolytes. Also, both the graphene-Be₂C₅ composite anode and pure Be₂C₅ anode upon potassiation possessed good mechanical strength. Not only that, the inevitable defects in the Be₂C₅ monolayer did not hinder its viability as a high-performance anode. As such, the Be₂C₅ monolayer is a potential candidate as an anode material for KIBs, with superior performance compared to existing 2D materials.

ACKNOWLEDGMENTS

We thank Professor Zhongfang Chen from the University of Puerto Rico and Guochun Yang from Yanshan University for valuable discussions. The authors acknowledge funding support from the National Natural Science Foundation of China (Grants No. T2225013, No. 12074154, No. 11904142, and No. 11722433), the Six Talent Peaks Project, the 333 High-Level Talents Project of Jiangsu Province, and the Postgraduate Research & Practice Innovation Program of Jiangsu Normal University (Grant No. 2022XKT1322). Computational resources have been provided by the High-Performance Computing Center of School of Physics and Electronic Engineering of Jiangsu Normal University.

-
- [1] D. Larcher and J. M. Tarascon, Towards greener and more sustainable batteries for electrical energy storage, *Nat. Chem.* **7**, 19 (2015).
 - [2] B. Dunn, H. Kamath, and J. M. Tarascon, Electrical energy storage for the grid: A battery of choices, *Science* **334**, 928 (2011).
 - [3] K. Chayambuka, G. Mulder, D. L. Danilov, and P. H. L. Notten, From Li-ion batteries toward Na-ion chemistries: Challenges and opportunities, *Adv. Energy Mater.* **10**, 2001310 (2020).

- [4] G. Abbas, S. M. Alay-e-Abbas, A. Laref, Y. Li, and W. X. Zhang, Two-dimensional B_3P monolayer as a superior anode material for Li and Na ion batteries: A first-principles study, *Mater. Today Energy* **17**, 100486 (2020).
- [5] C. Y. Zhu, X. Qu, M. Zhang, J. Y. Wang, Q. Li, Y. Geng, Y. M. Ma, and Z. M. Su, Planar NiC_3 as a reversible anode material with high storage capacity for lithium-ion and sodium-ion batteries, *J. Mater. Chem. A* **7**, 13356 (2019).
- [6] L. Shao, X. Y. Duan, Y. Li, F. G. Zeng, H. G. Ye, C. A. X. Su, and P. Ding, Two-dimensional planar BGe monolayer as an anode material for sodium-ion batteries, *ACS Appl. Mater. Interfaces* **13**, 29764 (2021).
- [7] D. S. Wang, Y. H. Liu, X. Meng, Y. J. Wei, Y. Y. Zhao, Q. Pang, and G. Chen, Two-dimensional VS_2 monolayers as potential anode materials for lithium-ion batteries and beyond: First-principles calculations, *J. Mater. Chem. A* **5**, 21370 (2017).
- [8] H. Gao, L. Xue, S. Xin, and J. B. Goodenough, A high-energy-density potassium battery with a polymer-gel electrolyte and a polyaniline cathode, *Angew. Chem., Int. Ed.* **57**, 5449 (2018).
- [9] T. Hosaka, K. Kubota, A. S. Hameed, and S. Komaba, Research development on K-ion batteries, *Chem. Rev.* **120**, 6358 (2020).
- [10] M. Sha, L. Liu, H. Zhao, and Y. Lei, Anode materials for potassium-ion batteries: Current status and prospects, *Carbon Energy* **2**, 350 (2020).
- [11] E. Olsson, J. Yu, H. Zhang, H. M. Cheng, and Q. Cai, Atomic-scale design of anode materials for alkali metal (Li/Na/K)-ion batteries: Progress and perspectives, *Adv. Energy Mater.* **12**, 2200662 (2022).
- [12] S. Liu, L. Kang, J. Henzie, J. Zhang, J. Ha, M. A. Amin, M. S. A. Hossain, S. C. Jun, and Y. Yamauchi, Recent advances and perspectives of battery-type anode materials for potassium ion storage, *ACS Nano* **15**, 18931 (2021).
- [13] Yuhan Wu, Yang Xu, Yueliang Li, Pengbo Lyu, Jin Wen, Chenglin Zhang, Min Zhou, Yaoguo Fang, Huaping Zhao, Ute Kaiser, and Yong Lei, Unexpected intercalation-dominated potassium storage in WS_2 as a potassium-ion battery anode, *Nano Res.* **12**, 2997 (2019).
- [14] J. Sheng, T. Wang, J. Tan, W. Lv, L. Qiu, Q. Zhang, G. Zhou, and H.-M. Cheng, Intercalation-induced conversion reactions give high-capacity potassium storage, *ACS Nano* **14**, 14026 (2020).
- [15] Chao Yang, Jianrui Feng, Fan Lv, Jinhui Zhou, Chunfu Lin, Kai Wang, Yelong Zhang, Yong Yang, Wei Wang, Jianbao Li, and Shaojun Guo, Metallic graphene-like VSe_2 ultrathin nanosheets: Superior potassium-ion storage and their working mechanism, *Adv. Mater.* **30**, 1800036 (2018).
- [16] S. Imtiaz, I. S. Amiinu, Y. Xu, T. Kennedy, C. Blackman, and K. M. Ryan, Progress and perspectives on alloying-type anode materials for advanced potassium-ion batteries, *Mater. Today* **48**, 241 (2021).
- [17] L. Wang, B. Zhang, B. Wang, S. Zeng, M. Zhao, X. Sun, Y. Zhai, and L. Xu, *In-situ* nano-crystallization and solvation modulation to promote highly stable anode involving alloy/de-alloy for potassium ion batteries, *Angew. Chem., Int. Ed.* **60**, 15381 (2021).
- [18] C. Li, A. T. Bi, H. L. Chen, Y. R. Pei, M. Zhao, C. C. Yang, and Q. Jiang, Rational design of porous Sn nanospheres/N-doped carbon nanofibers as an ultra-stable potassium-ion battery anode material, *J. Mater. Chem. A* **9**, 5740 (2021).
- [19] L. Fan, Y. Hu, A. M. Rao, J. Zhou, Z. Hou, C. Wang, and B. Lu, Prospects of electrode materials and electrolytes for practical potassium-based batteries, *Small Methods* **5**, 2101131 (2021).
- [20] Yanhong Feng, Yawei Lv, Hongwei Fu, Mihir Parekh, Apparao M Rao, He Wang, Xiaolin Tai, Xianhui Yi, Yue Lin, Jiang Zhou, and Bingan Lu, Co-activation for enhanced K-ion storage in battery anodes, *Natl. Sci. Rev.* **10**, nwad118 (2023).
- [21] H. Ding, J. Wang, J. Zhou, C. Wang, and B. Lu, Building electrode skins for ultra-stable potassium metal batteries, *Nat. Commun.* **14**, 2305 (2023).
- [22] Y. Y. Shi, G. J. Liu, R. C. Jin, H. Xu, Q. Y. Wang, and S. M. Gao, Carbon materials from melamine sponges for supercapacitors and lithium battery electrode materials: A review, *Carbon Energy* **1**, 253 (2019).
- [23] D. Q. Er, J. W. Li, M. Naguib, Y. Gogotsi, and V. B. Shenoy, Ti_3C_2 MXene as a high capacity electrode material for metal (Li, Na, K, Ca) ion batteries, *ACS Appl. Mater. Interfaces* **6**, 11173 (2014).
- [24] D. Çakır, C. Sevik, O. Gülsen, and F. M. Peeters, Mo_2C as a high capacity anode material: A first-principles study, *J. Mater. Chem. A* **4**, 6029 (2016).
- [25] J. Hu, B. Xu, C. Ouyang, Y. Zhang, and S. A. Yang, Investigations on Nb_2C monolayer as promising anode material for Li or non-Li ion batteries from first-principles calculations, *RSC Adv.* **6**, 27467 (2016).
- [26] J. Rehman, X. F. Fan, A. Laref, V. A. Dinh, and W. T. Zheng, Potential anodic applications of 2D MoS_2 for K-ion batteries, *J. Alloys Compd.* **865**, 158782 (2021).
- [27] A. Samad, A. Shafique, and Y.-H. Shin, Adsorption and diffusion of mono, di, and trivalent ions on two-dimensional TiS_2 , *Nanotechnology* **28**, 175401 (2017).
- [28] M. Tang, U. Schwingenschlögl, and G. Yang, The metallic C_6S monolayer with high specific capacity for K-ion batteries, *Mater. Today Chem.* **25**, 100951 (2022).
- [29] J. J. Jin, G. Deokar, P. Costa, and U. Schwingenschlögl, Monolayer C_5N : A Promising Building Block for the Anode of K-Ion Batteries, *Phys. Rev. Appl.* **17**, 034055 (2022).
- [30] C. Zhou, J. Huang, and X. Duan, Two-dimensional PC_3 as a promising anode material for potassium-ion batteries: First-principles calculations, *Chin. Phys. B* **30**, 056801 (2021).
- [31] L. J. Zhao, Y. Li, G. Y. Zhou, S. L. Lei, J. L. Tan, L. X. Lin, and J. J. Wang, First-principles calculations of stability of graphene-like BC_3 monolayer and its high-performance potassium storage, *Chin. Chem. Lett.* **32**, 900 (2021).
- [32] U. Younis, I. Muhammad, F. Qayyum, W. Wu, and Q. Sun, Two-dimensional metallic pentadiamond as anode material for Li-/Na-/K-ion batteries with high performance, *Mater. Today Energy* **20**, 100664 (2021).
- [33] M. Tang, C. Wang, U. Schwingenschlögl, and G. Yang, BC_6P Monolayer: Isostructural and isoelectronic

- analogues of graphene with desirable properties for K-ion batteries, *Chem. Mater.* **33**, 9262 (2021).
- [34] X. Guan, H. Song, Y. Tang, X. Zhong, J. Wang, J. Cheng, and D. Zou, Theory prediction of PC₃ monolayer as a promising anode material in potassium-ion batteries, *Ionics* **27**, 2465 (2021).
- [35] U. Younis, I. Muhammad, Y. Kawazoe, and Q. Sun, Design of tetracene-based metallic 2D carbon materials for Na-and K-ion batteries, *Appl. Surf. Sci.* **521**, 146456 (2020).
- [36] Y. Wang and Y. Li, *Ab initio* prediction of two-dimensional Si₃C enabling high specific capacity as an anode material for Li/Na/K-ion batteries, *J. Mater. Chem. A* **8**, 4274 (2020).
- [37] J. Rehman, X. Fan, A. Laref, and W. Zheng, Adsorption and diffusion of potassium on 2D SnC sheets for potential high-performance anodic applications of potassium-ion batteries, *ChemElectroChem* **7**, 3832 (2020).
- [38] Y. Ding, Q. Deng, C. You, Y. Xu, J. Li, and B. Xiao, Assessing electrochemical properties and diffusion dynamics of metal ions (Na, K, Ca, Mg, Al and Zn) on a C₂N monolayer as an anode material for non-lithium ion batteries, *Phys. Chem. Chem. Phys.* **22**, 21208 (2020).
- [39] Y. Chu, K. Yeoh, and K.-H. Chew, A first-principles comparative study of lithium, sodium, potassium and calcium storage in two-dimensional Mg₂C, *J. Phys.: Condens. Matter* **33**, 075002 (2020).
- [40] Q. Chen, H. Wang, H. Li, Q. Duan, D. Jiang, and J. Hou, Two-dimensional MnC as a potential anode material for Na/K-ion batteries: A theoretical study, *J. Mol. Model.* **26**, 66 (2020).
- [41] I. Muhammad, S. Wang, J. Liu, H. Xie, and Q. Sun, Boron-graphdiyne as an anode material for Li, Na, and K ion batteries with high capacities and low diffusion barriers, *J. Renewable Sustainable Energy* **11**, 014106 (2019).
- [42] K. Dou, Y. Ma, T. Zhang, B. Huang, and Y. Dai, Prediction of two-dimensional PC₆ as a promising anode material for potassium-ion batteries, *Phys. Chem. Chem. Phys.* **21**, 26212 (2019).
- [43] P. Bhauriyal, A. Mahata, and B. Pathak, Graphene-like carbon-nitride monolayer: A potential anode material for Na- and K-ion batteries, *J. Phys. Chem. C* **122**, 2481 (2018).
- [44] F. Li, X. Liu, J. Wang, X. Zhang, B. Yang, Y. Qu, and M. Zhao, A promising alkali-metal ion battery anode material: 2D metallic phosphorus carbide (β_0 -PC), *Electrochim. Acta* **258**, 582 (2017).
- [45] R. P. Joshi, B. Ozdemir, V. Barone, and J. E. Peralta, Hexagonal BC₃: A robust electrode material for Li, Na, and K ion batteries, *J. Phys. Chem. Lett.* **6**, 2728 (2015).
- [46] S. F. Lei, X. F. Chen, B. B. Xiao, W. T. Zhang, and J. Liu, Excellent electrolyte wettability and high energy density of B₂S as a two-dimensional Dirac anode for non-lithium-ion batteries, *ACS Appl. Mater. Interfaces* **11**, 28830 (2019).
- [47] P. Xiang, X. F. Chen, B. B. Xiao, and Z. M. Wang, Highly flexible hydrogen boride monolayers as potassium-ion battery anodes for wearable electronics, *ACS Appl. Mater. Interfaces* **11**, 8115 (2019).
- [48] S. Sun and X. Ye, Monolayer Be₂P₃N as a high capacity and high energy density anode material for ultrafast charging Na- and K-ion batteries, *Appl. Surf. Sci.* **527**, 146783 (2020).
- [49] S. F. Lei, X. F. Chen, J. W. Wen, X. Y. Zhou, and B. B. Xiao, Passivated 2D Janus borophene as unique Dirac anodes for Na- and K-ion batteries: A first-principle investigation, *Appl. Surf. Sci.* **578**, 151994 (2022).
- [50] H. Lin, G. J. Liu, L. L. Zhu, Z. J. Zhang, R. C. Jin, Y. Huang, and S. M. Gao, Flexible borophosphene monolayer: A potential Dirac anode for high-performance non-lithium ion batteries, *Appl. Surf. Sci.* **544**, 148895 (2021).
- [51] Z. S. Cheng, X. M. Zhang, H. Zhang, H. Y. Liu, X. Yu, X. F. Dai, G. D. Liu, and G. F. Chen, BeN₄ monolayer as an excellent Dirac anode material for potassium-ion batteries, *J. Alloys Compd.* **936**, 168351 (2023).
- [52] B. Tian, W. Du, L. Chen, J. Guo, H. Shu, Y. Wang, and J. Dai, Probing pristine and defective NiB₆ monolayer as promising anode materials for Li/Na/K ion batteries, *Appl. Surf. Sci.* **527**, 146580 (2020).
- [53] A. Sannayal, Y. Ahn, and J. Jang, First-principles study on the two-dimensional siligene (2D SiGe) as an anode material of an alkali metal ion battery, *Comput. Mater. Sci.* **165**, 121 (2019).
- [54] Y. Hu, Y. Liu, Y. Huang, and H. Lin, Flexible Si₃C monolayer: A superior anode for high-performance non-lithium ion batteries, *Colloids Surf., A* **637**, 128238 (2022).
- [55] P. Xiang, X. Chen, W. Zhang, J. Li, B. Xiao, L. Li, and K. Deng, Metallic borophene polytypes as lightweight anode materials for non-lithium-ion batteries, *Phys. Chem. Chem. Phys.* **19**, 24945 (2017).
- [56] H. Lin, L. Zhu, Z. Zhang, R. Jin, Y. Huang, and Y. Hu, Semi-metallic PC₅ monolayer as a superior anode material for potassium ion batteries: A first principles study, *Colloids Surf., A* **643**, 128756 (2022).
- [57] M. M. Obeid and Q. Sun, Recent advances in topological quantum anode materials for metal-ion batteries, *J. Power Sources* **540**, 231655 (2022).
- [58] Dewei Rao, Lingyan Zhang, Zhaoshun Meng, Xirui Zhang, Yunhui Wang, Guanjun Qiao, Xiangqian Shen, Hui Xia, Jiehua Liud, and Ruifeng Lu, Ultrahigh energy storage and ultrafast ion diffusion in borophene-based anodes for rechargeable metal ion batteries, *J. Mater. Chem. A* **5**, 2328 (2017).
- [59] Y. Wang, J. Lv, L. Zhu, and Y. Ma, Crystal structure prediction via particle-swarm optimization, *Phys. Rev. B* **82**, 094116 (2010).
- [60] Y. C. Wang, J. Lv, L. Zhu, and Y. M. Ma, CALYPSO: A method for crystal structure prediction, *Comput. Phys. Commun.* **183**, 2063 (2012).
- [61] Y. C. Wang, M. S. Miao, J. Lv, L. Zhu, K. T. Yin, H. Y. Liu, and Y. M. Ma, An effective structure prediction method for layered materials based on 2D particle swarm optimization algorithm, *J. Chem. Phys.* **137**, 224108 (2012).
- [62] B. Gao, P. Gao, S. Lu, J. Lv, Y. Wang, and Y. Ma, Interface structure prediction via CALYPSO method, *Sci. Bull.* **64**, 301 (2019).
- [63] X. Shao, J. Lv, P. Liu, S. Shao, P. Gao, H. Liu, Y. Wang, and Y. Ma, A symmetry-orientated divide-and-conquer

- method for crystal structure prediction, *J. Chem. Phys.* **156**, 014105 (2022).
- [64] M. Xu, C. Huang, Y. Li, S. Liu, X. Zhong, P. Jena, E. Kan, and Y. Wang, Electrical Control of Magnetic Phase Transition in a Type-I Multiferroic Double-Metal Trihalide Monolayer, *Phys. Rev. Lett.* **124**, 067602 (2020).
- [65] C. Tang, L. Zhang, S. Sanvito, and A. Du, Enabling room-temperature triferroic coupling in dual transition-metal dichalcogenide monolayers via electronic asymmetry, *J. Am. Chem. Soc.* **145**, 2485 (2023).
- [66] D. Chen, Y. Wang, and R. Dronskowski, Computational design and theoretical properties of WC₃N₆, an H-free melamine and potential multifunctional material, *J. Am. Chem. Soc.* **145**, 6986 (2023).
- [67] Xin Qu, Lihua Yang, Jian Lv, Yu Xie, Jinghai Yang, Yukai Zhang, Yanchao Wang, Jijun Zhao, Zhongfang Chen, and Yanming Ma, Particle swarm predictions of a SrB₈ monolayer with 12-fold metal coordination, *J. Am. Chem. Soc.* **144**, 11120 (2022).
- [68] J. Feng, Z. Dong, Y. Ji, and Y. Li, Accelerating the discovery of metastable IrO₂ for the oxygen evolution reaction by the self-learning-input graph neural network, *JACS Au* **3**, 1131 (2023).
- [69] T. Yu, Z. Zhao, L. Liu, S. Zhang, H. Xu, and G. Yang, TiC₃ monolayer with high specific capacity for sodium-ion batteries, *J. Am. Chem. Soc.* **140**, 5962 (2018).
- [70] G. Kresse and J. Furthmüller, Efficient iterative schemes for ab initio total-energy calculations using a plane-wave basis set, *Phys. Rev. B* **54**, 11169 (1996).
- [71] J. P. Perdew, K. Burke, and M. Ernzerhof, Generalized Gradient Approximation Made Simple, *Phys. Rev. Lett.* **77**, 3865 (1996).
- [72] G. Kresse and D. Joubert, From ultrasoft pseudopotentials to the projector augmented-wave method, *Phys. Rev. B* **59**, 1758 (1999).
- [73] A. Togo and I. Tanaka, First principles phonon calculations in materials science, *Scr. Mater.* **108**, 1 (2015).
- [74] S. Grimme, S. Ehrlich, and L. Goerigk, Effect of the damping function in dispersion corrected density functional theory, *J. Comput. Chem.* **32**, 1456 (2011).
- [75] G. Henkelman, B. P. Uberuaga, and H. Jonsson, A climbing image nudged elastic band method for finding saddle points and minimum energy paths, *J. Chem. Phys.* **113**, 9901 (2000).
- [76] G. Henkelman and H. Jonsson, Improved tangent estimate in the nudged elastic band method for finding minimum energy paths and saddle points, *J. Chem. Phys.* **113**, 9978 (2000).
- [77] See the Supplemental Material at <http://link.aps.org/supplemental/10.1103/PRXEnergy.2.033012> for computational details on the direction-dependent Young's modulus and Poisson's ratio, Fermi velocity, adsorption energy, temperature-dependent molecular diffusion constant, OCV, formation energy, specific capacity, and lattice change rate; phonon dispersion curves, MD simulations, structural information, and elastic constants of the Be₂C₅ monolayer; DOS and MD simulations of Be₂C₅K_x ($x = 2, 4$, and 6) phases; summaries of the diffusion barrier, specific capacity, OCV, and energy density of representative 2D anode material candidates as KIBs; stress-strain curves of the pure Be₂C₅ and graphene/Be₂C₅ anodes; crystal structures of electrolytes adsorbed on the Be₂C₅ surface; and POSCARs for Be₂C₅K_x ($x = 2, 4$, and 6) phases; it also includes Refs. [7,23–56,58,78–102].
- [78] Y. Hu, J. Wang, and H. Lin, Metallic two-dimensional P₂C₃: A promising flexible anode for high-performance potassium-ion batteries, *Colloids Surf., A* **619**, 126536 (2021).
- [79] P. Xiang, S. Sharma, Z. M. Wang, J. Wu, and U. Schwingenschlögl, Flexible C₆BN monolayers as promising anode materials for high-performance K-ion batteries, *ACS Appl. Mater. Interfaces* **12**, 30731 (2020).
- [80] M. Sun, Y. Yan, and U. Schwingenschlögl, Beryllene: A promising anode material for Na- and K-ion batteries with ultrafast charge/discharge and high specific capacity, *J. Phys. Chem. Lett.* **11**, 9051 (2020).
- [81] Z. Jian, W. Luo, and X. Ji, Carbon electrodes for K-ion batteries, *J. Am. Chem. Soc.* **137**, 11566 (2015).
- [82] B. Xu, H.-S. Lu, B. Liu, G. Liu, M.-S. Wu, and C. Ouyang, Comparisons between adsorption and diffusion of alkali, alkaline earth metal atoms on silicene and those on silicane: Insight from first-principles calculations, *Chin. Phys. B* **25**, 067103 (2016).
- [83] A. Sibari, Z. Kerrami, A. Kara, M. Hamedoun, A. Benyoussef, O. Mounkachi, and M. Benaissa, Adsorption and diffusion on a phosphorene monolayer: A DFT study, *J. Solid State Electrochem.* **22**, 11 (2018).
- [84] I. Sultana, M. M. Rahman, T. Ramireddy, Y. Chen, and A. M. Glushenkov, High capacity potassium-ion battery anodes based on black phosphorus, *J. Mater. Chem. A* **5**, 23506 (2017).
- [85] S. Mukherjee, L. Kavalsky, and C. V. Singh, Ultrahigh storage and fast diffusion of Na and K in blue phosphorene anodes, *ACS Appl. Mater. Interfaces* **10**, 8630 (2018).
- [86] Y. Dong, Z. Tang, P. Liang, H. Wan, H. Wang, L. Wang, H. Shu, and D. Chao, 2D-VN₂ MXene as a novel anode material for Li, Na and K ion batteries: Insights from the first-principles calculations, *J. Colloid Interface Sci.* **593**, 51 (2021).
- [87] S. Gong, C. Zhang, S. Wang, and Q. Wang, Ground-state structure of YN₂ monolayer identified by global search, *J. Phys. Chem. C* **121**, 10258 (2017).
- [88] S.-H. Zhang and B.-G. Liu, Superior ionic and electronic properties of ReN₂ monolayers for Na-ion battery electrodes, *Nanotechnology* **29**, 325401 (2018).
- [89] Junhua Zhou, Lu Wang, Mingye Yang, Jinghua Wu, Fengjiao Chen, Wenjing Huang, Na Han, Hualin Ye, Feipeng Zhao, Youyong Li, and Yanguang Li, Hierarchical VS₂ nanosheet assemblies: A universal host material for the reversible storage of alkali metal ions, *Adv. Mater.* **29**, 1702061 (2017).
- [90] Y. Shen, J. Liu, X. Li, and Q. Wang, Two-dimensional T-NiSe₂ as a promising anode material for potassium-ion batteries with low average voltage, high ionic conductivity, and superior carrier mobility, *ACS Appl. Mater. Interfaces* **11**, 35661 (2019).
- [91] H. R. Jiang, W. Shyy, M. Liu, L. Wei, M. C. Wu, and T. S. Zhao, Boron phosphide monolayer as a potential anode material for alkali metal-based batteries, *J. Mater. Chem. A* **5**, 672 (2017).

- [92] S. Ullah, P. A. Denis, and F. Sato, Monolayer boron-arsenide as a perfect anode for alkali-based batteries with large storage capacities and fast mobilities, *Int. J. Quantum Chem.* **119**, e25975 (2019).
- [93] N. Khossossi, A. Banerjee, Y. Benhouria, I. Essaoudi, A. Ainane, and R. Ahuja, *Ab initio* study of a 2D *h*-BAs monolayer: A promising anode material for alkali-metal ion batteries, *Phys. Chem. Chem. Phys.* **21**, 18328 (2019).
- [94] F. Li, Y. Qu, and M. Zhao, Germanium sulfide nanosheet: A universal anode material for alkali metal ion batteries, *J. Mater. Chem. A* **4**, 8905 (2016).
- [95] Y. Zhou, M. Zhao, Z. W. Chen, X. M. Shi, and Q. Jiang, Potential application of 2D monolayer β -GeSe as an anode material in Na/K ion batteries, *Phys. Chem. Chem. Phys.* **20**, 30290 (2018).
- [96] J. Rehman, X. Fan, and W. Zheng, Computational insight of monolayer SnS₂ as anode material for potassium ion batteries, *Appl. Surf. Sci.* **496**, 143625 (2019).
- [97] J. Rehman, X. Fan, M. Butt, A. Laref, V. A. Dinh, and W. Zheng, First principles predictions of Na and K storage in layered SnSe₂, *Appl. Surf. Sci.* **566**, 150522 (2021).
- [98] X. Lv, F. Li, J. Gong, J. Gu, S. Lin, and Z. Chen, Metallic FeSe monolayer as an anode material for Li and non-Li ion batteries: A DFT study, *Phys. Chem. Chem. Phys.* **22**, 8902 (2020).
- [99] Yuanzheng Chen, Haifei Qin, Jun Zhou, Tong Yang, Bai Sun, Yuxiang Ni, Hongyan Wang, Simon A. T. Redfern, Maosheng Miao, Hai-Qing Lin, and Yuan Ping Feng, Unveiling interstitial anionic electron-driven ultrahigh K-ion storage capacity in a novel two-dimensional electride exemplified by Sc₃Si₂, *J. Phys. Chem. Lett.* **13**, 7439 (2022).
- [100] A. Sannyal, Z. Zhang, X. Gao, and J. Jang, Two-dimensional sheet of germanium selenide as an anode material for sodium and potassium ion batteries: First-principles simulation study, *Comput. Mater. Sci.* **154**, 204 (2018).
- [101] E. Cadelano, P. L. Palla, S. Giordano, and L. Colombo, Elastic properties of hydrogenated graphene, *Phys. Rev. B* **82**, 235414 (2010).
- [102] X. M. Zhang, Z. M. Yu, S. S. Wang, S. Guan, H. Y. Yang, Y. G. Yao, and S. Y. A. Yang, Theoretical prediction of MoN₂ monolayer as a high capacity electrode material for metal ion batteries, *J. Mater. Chem. A* **4**, 15224 (2016).
- [103] K. S. Novoselov, A. K. Geim, S. V. Morozov, D. Jiang, Y. Zhang, S. V. Dubonos, I. V. Grigorieva, and A. A. Firsov, Electric field effect in atomically thin carbon films, *Science* **306**, 666 (2004).
- [104] A. D. Becke and K. E. Edgecombe, A simple measure of electron localization in atomic and molecular systems, *J. Chem. Phys.* **92**, 5397 (1990).
- [105] G. Henkelman, A. Arnaldsson, and H. Jonsson, A fast and robust algorithm for Bader decomposition of charge density, *Comput. Mater. Sci.* **36**, 354 (2006).
- [106] F. Mouhat and F.-X. Coudert, Necessary and sufficient elastic stability conditions in various crystal systems, *Phys. Rev. B* **90**, 224104 (2014).
- [107] C. Lee, X. Wei, J. W. Kysar, and J. Hone, Measurement of the elastic properties and intrinsic strength of monolayer graphene, *Science* **321**, 385 (2008).
- [108] R. C. Andrew, R. E. Mapasha, A. M. Ukpong, and N. Chetty, Mechanical properties of graphene and boronitrene, *Phys. Rev. B* **85**, 125428 (2012).
- [109] Y. Ding and Y. Wang, Density functional theory study of the silicene-like SiX and XSi₃ (X = B, C, N, Al, P) honeycomb lattices: The various buckled structures and versatile electronic properties, *J. Phys. Chem. C* **117**, 18266 (2013).
- [110] R. C. Cooper, C. Lee, C. A. Marianetti, X. Wei, J. Hone, and J. W. Kysar, Nonlinear elastic behavior of two-dimensional molybdenum disulfide, *Phys. Rev. B* **87**, 035423 (2013).
- [111] Meiling Xu, Guohui Zhan, Siyu Liu, Dongqin Zhang, Xin Zhong, Ziyang Qu, Yinwei Li, Aijun Du, Haijun Zhang, and Yanchao Wang, PT-symmetry-protected Dirac states in strain-induced hidden MoS₂ monolayer, *Phys. Rev. B* **100**, 235435 (2019).
- [112] J. K. Lyu, W. X. Ji, S. F. Zhang, C. W. Zhang, and P. J. Wang, Two-dimensional honeycomb B₂Se with orthogonal lattice: High stability and strong anisotropic Dirac cone, *J. Phys. Chem. C* **124**, 7558 (2020).
- [113] Y. Zhao, X. Li, J. Liu, C. Zhang, and Q. Wang, A new anisotropic Dirac cone material: A B₂S honeycomb monolayer, *J. Phys. Chem. Lett.* **9**, 1815 (2018).
- [114] Y. Zhang, J. Kang, F. Zheng, P.-F. Gao, S.-L. Zhang, and L.-W. Wang, Borophosphene: A new anisotropic Dirac cone monolayer with a high Fermi velocity and a unique self-doping feature, *J. Phys. Chem. Lett.* **10**, 6656 (2019).
- [115] J. Heyd, G. E. Scuseria, and M. Ernzerhof, Hybrid functionals based on a screened Coulomb potential, *J. Chem. Phys.* **118**, 8207 (2003).
- [116] D. Malko, C. Neiss, F. Viñes, and A. Görling, Competition for Graphene: Graphynes with Direction-Dependent Dirac Cones, *Phys. Rev. Lett.* **108**, 086804 (2012).
- [117] J. Dahn, Phase diagram of Li_xC₆, *Phys. Rev. B* **44**, 9170 (1991).
- [118] Y. Cao, M. Li, J. Lu, J. Liu, and K. Amine, Bridging the academic and industrial metrics for next-generation practical batteries, *Nat. Nanotechnol.* **14**, 200 (2019).
- [119] W. Li, X. Sun, and Y. Yu, Si-,Ge-,Sn-based anode materials for lithium-ion batteries: From structure design to electrochemical performance, *Small Methods* **1**, 1600037 (2017).
- [120] Jian Yu Huang, Li Zhong, Chong Min Wang, John P Sullivan, Wu Xu, Li Qiang Zhang, Scott X Mao, Nicholas S Hudak, Xiao Hua Liu, Arunkumar Subramanian, Hongyou Fan, Liang Qi, Akihiro Kushima, and Ju Li, *In situ* observation of the electrochemical lithiation of a single SnO₂ nanowire electrode, *Science* **330**, 1515 (2010).
- [121] X. H. Liu, *et al.*, Anisotropic swelling and fracture of silicon nanowires during lithiation, *Nano Lett.* **11**, 3312 (2011).
- [122] D. H. Jeon, Wettability in electrodes and its impact on the performance of lithium-ion batteries, *Energy Storage Mater.* **18**, 139 (2019).
- [123] J. Li, Y. Hu, H. Xie, J. Peng, L. Fan, J. Zhou, and B. Lu, Weak cation–solvent interactions in ether-based electrolytes stabilizing potassium-ion batteries, *Angew. Chem., Int. Ed.* **61**, e202208291 (2022).

- [124] H. Zhao, J. Xu, D. Yin, and Y. Du, Electrolytes for batteries with Earth-abundant metal anodes, *Chem. - Eur. J.* **24**, 18220 (2018).
- [125] Q. Zhang, J. Mao, W. K. Pang, T. Zheng, V. Sencadas, Y. Chen, Y. Liu, and Z. Guo, Boosting the potassium storage performance of alloy-based anode materials via electrolyte salt chemistry, *Adv. Energy Mater.* **8**, 1703288 (2018).
- [126] Y. Wang, F. Li, Y. F. Li, and Z. F. Chen, Semi-metallic Be₅C₂ monolayer global minimum with quasi-planar pentacoordinate carbons and negative Poisson's ratio, *Nat. Commun.* **7**, 11488 (2016).